Spin-orbital model of stoichiometric $LaMnO_3$ with tetragonal distortions

Mateusz Snamina[1] and Andrzej M. Oleś[2,3]
[1]*Kazimierz Gumiński Department of Theoretical Chemistry, Faculty of Chemistry, Jagiellonian University, Gronostajowa 2, PL-30387 Kraków, Poland*
[2]*Marian Smoluchowski Institute of Physics, Faculty of Physics, Astronomy, and Applied Computer Science, Jagiellonian University, Prof. S. Łojasiewicza 11, PL-30348 Kraków, Poland*
[3]*Max Planck Institute for Solid State Research, Heisenbergstrasse 1, D-70569 Stuttgart, Germany*

(Received 12 September 2017; revised manuscript received 3 January 2018; published 23 March 2018)

The spin-orbital superexchange model is derived for the cubic (perovskite) symmetry of $LaMnO_3$, whereas real crystal structure is strongly deformed. We identify and explain three *a priori* important physical effects arising from tetragonal deformation: (i) the splitting of e_g orbitals $\propto E_z$, (ii) the directional renormalization of d-p hybridization t_{pd}, and (iii) the directional renormalization of charge excitation energies. Using the example of $LaMnO_3$ crystal we evaluate their magnitude. It is found that the major effects of deformation are an enhanced amplitude of x^2-y^2 orbitals induced in the orbital order by $E_z \simeq 300$ meV and anisotropic $t_{pd} \simeq 2.0$ (2.35) eV along the ab (c) cubic axis, in very good agreement with Harrison's law. We show that the improved tetragonal model analyzed within mean field approximation provides a surprisingly consistent picture of the ground state. Excellent agreement with the experimental data is obtained simultaneously for: (i) e_g orbital mixing angle, (ii) spin exchange constants, and (iii) the temperatures of spin and orbital phase transition.

DOI: 10.1103/PhysRevB.97.104417

I. INTRODUCTION

Manganites, cuprates, and vanadates are wide groups of compounds that have been attracting much attention, both theoretical and experimental. What makes them intriguing are strong electron correlations that cause electron localization [1] and thus lead to effective superexchange models with quantum behavior of coexisting spin and orbital degrees of freedom [2]. Theoretical description is even more demanding due to structural phase transitions. To capture low energy phenomena at strong correlations, superexchange models were were extended by effective orbital interactions induced by the Jahn-Teller (JT) effect [3,4]. Realistic models employ the parameters derived from *ab initio* calculations or from experiment and thus serve as satisfactory and convincing explanation of interactions in the space of spin-orbital degrees of freedom [5,6]. Several nontrivial disordered [7,8] or ordered [9] phases arise as a generic consequence of spin-orbital exchange interactions, including novel phases found by orbital [10] or charge [11] dilution. Though such models have been successful in working out the peculiar physical properties of doped manganites [12,13], the structural aspects have usually been neglected. One of them is the interplay between a crystal geometry and the actual spin-orbital interactions.

Except for cuprate superconductors [14,15], one of the physical aspects of perovskites that has not yet been fully investigated is a shortening of some bonds in the crystal structure and elongation of the others. Any deformation of the crystal results in the lowering of lattice symmetry from cubic to tetragonal. In this paper we are peering at this structural aspect in detail. We choose $LaMnO_3$ as a guide compound as it is described in many textbooks and the spin-orbital superexchange model [16] is well known and has been employed to explain the temperature dependence of the spectral weights observed in the optical spectroscopy [17]. Hund's exchange stabilizes large spins $S = 2$ in $LaMnO_3$ and quantum effects are then reduced. Thus spin-orbital entanglement is small as we have shown in a recent study [18]. Then an additional advantage is that the analysis is simpler here than for some systems with smaller spins (such as $S = 1/2$ in $KCuF_3$) where spin-orbital entanglement cannot be neglected [19,20] as spin and orbital degrees of freedom strongly influence each other. However, superexchange alone is not sufficient to explain the high value of the orbital transition temperature T_{OO} [16,21–23]. A careful study of the orbital melting transition suggests that superexchange interactions play a minor role for this transition while tetragonal crystal-field (CF) splitting E_z has to be included to explain experiments [24]. Also in high-T_c cuprates important changes of the microscopic parameters such as the orbital splitting [14] and p-d hybridization [15] follow from the tetragonal geometry. This motivates us to go beyond the cubic model and to evaluate E_z and the anisotropy in t_{pd} for $LaMnO_3$.

Indeed, the real $LaMnO_3$ crystal structure is much more complicated than that of an ideal cubic perovskite. It may be perceived as a cubic perovskite with one period, i.e., bond length in antiferromagnetic (AF) c direction is significantly shorter than the ferromagnetic (FM) bonds along a and b axes (with the difference between them of about 3.5% of the initial length). This tetragonal deformation is thus *opposite* to that found in high-T_c cuprates, where the apical oxygens are more distant from $3d$ ions than the oxygens in the ab planes, as predicted by the electronic structure calculations [25] and confirmed experimentally [26]. In addition, MnO_6 octahedra are slightly tilted (so that the space group is *Pmna*). In this work we modify the cubic model so that it takes into account the

differences of period lengths but completely neglects octahedra tilts. We show below that the period lengths difference is related to the orbital state. The bigger the lengths difference is, the more robust the orbital state becomes. For this reason the onset of an orbital order takes place simultaneously with a structural phase transition [26–28].

In our previous work [18] we concentrated on the influence of the diverse spin-orbital entanglements (i.e., on-site and on-bond entanglement) on the electronic state of the $LaMnO_3$ crystal. The goal of the present work is to assess the influence of the crystal tetragonal deformation and to identify the main underlying physical mechanisms playing a role for realistic description. As the $LaMnO_3$ crystal is a representative compound that is described by the Kugel-Khomskii-like model that undergoes strong JT effect, we argue that the present considerations may be treated as a guideline for any similar model extensions for analogous crystals.

Key degrees of freedom of the $LaMnO_3$ crystal are associated with manganese ions. They have $3d^4$ high-spin (HS) $t_{2g}^3 e_g^1$ configuration with spin $S = 2$. Thus each manganese ion has a large magnetic moment that may point at any direction [due to SU(2) symmetry]. In addition to the magnetic degree of freedom there is an orbital one due to a single e_g electron. As every manganese ion is at a center of a (slightly deformed) MnO_6 octahedron, its $3d$ orbitals are split and the HS d^4 configuration includes the occupied e_g orbital with lower energy. The e_g electron occupies, in general, at site i a linear combination of two basis states [29],

$$|i\vartheta\rangle = \cos(\vartheta/2)|i\zeta_c\rangle + \sin(\vartheta/2)|i\xi_c\rangle, \tag{1}$$

where the orbital basis consists of the two basis orbitals (labeled in analogy to $|\uparrow\rangle$ and $|\downarrow\rangle$ spin states):

$$|\zeta_c\rangle \equiv \tfrac{1}{\sqrt{6}}(3z^2 - r^2), \quad |\xi_c\rangle \equiv \tfrac{1}{\sqrt{2}}(x^2 - y^2), \tag{2}$$

a directional orbital $|\zeta_c\rangle$ along the c axis, and an orthogonal to its planar orbital $|\xi_c\rangle$. The orbital basis states in Eq. (2) are obtained for $\vartheta = 0$ and $\vartheta = \pi$, respectively, while for angles increased by $2\pi/3$ or $4\pi/3$ two other equivalent pairs of states are obtained: $\{\zeta_a,\xi_a\}$ and $\{\zeta_b,\xi_b\}$. The orbital state at site i (1) is parametrized by an *orbital mixing angle* $\vartheta \in [0,2\pi)$. Thus the state at each manganese ion is described by the direction of its spin projection and the angle ϑ. A 3D cubic lattice of manganese ions in the $LaMnO_3$ crystal may just be viewed as a set consisting of the above pairs of variables, representing the degrees of freedom of each ion in the lattice.

The spin order in the ground state of the $LaMnO_3$ crystal is A-type AF (A-AF). It means that the crystal is made of FM ab planes that are staggered in an AF manner along the c axis. The orbital state is nontrivial as well. The manganese's e_g electron states are equal to $|\pm\vartheta\rangle$, where the angle $\vartheta \in [0,\pi)$ takes for some fixed value and the sign alternates between the A and B sublattice in each ab plane [6]. The orbital state is unchanged along the perpendicular c axis, i.e., the alternating orbital (AO) order is C type labeled as C-AO.

The purpose of this paper is to introduce and investigate the consequences of the tetragonal crystal structure of $LaMnO_3$ which takes into account the experimental distortions. It is noteworthy that the cubic model predicts the reduction of symmetry in the ordered state as one direction is distinguished by the spin-orbital order (the AF direction in A-AF/C-AO state). In this state the symmetry is broken, i.e., the ground state has lower symmetry than the symmetry of the model itself. On the contrary, the proposed tetragonal model has lower symmetry from the beginning. Following the observed structure [31], in this work we label the "shortened" AF directions by the letter c, and the "elongated" FM directions a and b.

The paper is organized as follows. In Sec. II we develop a spin-orbital model for $LaMnO_3$ in the tetragonal phase. We begin with recalling the model for the usually considered cubic structure in Sec. II A, present the tetragonal structure in Sec. II B, and summarize the necessary changes in Sec. II C. In Sec. III we concentrate on the tetragonal crystal field (CF): (i) introduce its microscopic description in Sec. III A, (ii) present its consequences on the ground state in Sec. III B, and (iii) determine the actual value of the e_g orbital splitting by an *ab initio* approach in Sec. III C. The lattice distortions in $LaMnO_3$ lead to the renormalized superexchange model presented in Sec. IV. We begin with recalling the perturbative origin of the spin-orbital model in Sec. IV A and then discuss the renormalization of both hybridization t_{pd} hopping elements and charge excitation energies in Secs. IV B and IV C. The predictions of the tetragonal model at $T = 0$ are given in Sec. V A, and next discussed in Sec. V B. As the tetragonal distortion changes together with the electronic state, the predictions of the model at finite temperature are distinct from those of the cubic model as we show in the Appendix. Finally we present the main conclusions and summarize the present study in Sec. VI.

II. TETRAGONAL MODEL FOR $LaMnO_3$

A. Spin-orbital model for cubic $LaMnO_3$

In the previous works the $LaMnO_3$ crystal electronic structure was investigated with the aid of pure electronic superexchange Kugel-Khomskii-like models [16–18]. Typically, such models are formulated in terms of the ionic spin-orbital degrees of freedom for Mn ions (all other degrees of freedom are integrated out, including degrees of freedom attributed to the bridge atoms). All terms in the superexchange Hamiltonian correspond to the ionic pairs on nearest neighbor bonds (denoted here as $\langle ij\rangle$).

Charge excitations responsible for superexchange arise from electron hopping t defined for e_g electrons as the largest hopping element for a σ bond $\langle ij\rangle \parallel \gamma$, i.e., between two active orbitals, $|i\zeta_\gamma\rangle$ and $|j\zeta_\gamma\rangle$ along this bond. In the cubic crystal t is independent of the bond direction γ. In the regime of large intraorbital Coulomb repulsion $U \gg t$, one can construct the low-energy Hamiltonian by attributing each virtual excitation numerated by subscript n with the Hamiltonian contribution,

$$H_n^\gamma(ij) = (a_n + b_n \vec{S}_i \cdot \vec{S}_j)\mathcal{Q}_n^\gamma(ij), \tag{3}$$

where a_n and b_n are numeric coefficients derived from the multiband extended Hubbard model; the explicit form of the Hamiltonian was presented in Ref. [18]. Here $\{\vec{S}_i\}$ denotes the spin operator (for ith site) and $\mathcal{Q}_n^\gamma(ij)$ denotes the on-bond orbital operator, specifying the orbital configuration. It is expressed in terms of on-site orbital operators $\{\tau_i^{(\gamma)}\}$ (that explicitly depend on the crystallographic direction γ of the

$\langle ij\rangle$ bond):

$$\tau_i^{(a)} = -\frac{1}{4}\sigma_i^z - \frac{\sqrt{3}}{4}\sigma_i^x,$$
$$\tau_i^{(b)} = -\frac{1}{4}\sigma_i^z + \frac{\sqrt{3}}{4}\sigma_i^x,$$
$$\tau_i^{(c)} = \frac{1}{2}\sigma_i^z, \tag{4}$$

where σ_i^z and σ_i^x are Pauli matrices acting in the space spanned by the orbital basis Eq. (2) at site i.

A charge excitation between two transition metal ions with partly filled e_g orbitals will arise by a hopping process between two active orbitals $|i\zeta_\gamma\rangle$ and $|j\zeta_\gamma\rangle$. To capture the directional dependence of such processes we introduce two projection operators on the orbital states for each bond,

$$\mathcal{Q}_\perp^{(\gamma)}(ij) \equiv 2\left(\frac{1}{4} - \tau_i^{(\gamma)}\tau_j^{(\gamma)}\right), \tag{5}$$
$$\mathcal{Q}_\parallel^{(\gamma)}(ij) \equiv 2\left(\frac{1}{2} + \tau_i^{(\gamma)}\right)\left(\frac{1}{2} + \tau_j^{(\gamma)}\right). \tag{6}$$

Unlike for a spin system, the charge excitation $d_i^m d_j^m \rightleftharpoons d_i^{m+1} d_j^{m-1}$ is allowed only in one direction when one orbital is directional $|\zeta_\gamma\rangle$ and the other is planar $|\xi_{\gamma'}\rangle$ for a given bond $\langle ij\rangle \parallel \gamma$, i.e., $\langle \mathcal{Q}_\perp^{(\gamma)}(ij)\rangle = 1$; such processes generate both HS and low-spin (LS) contributions. On the contrary, when both orbitals are directional, i.e., one has $\langle \mathcal{Q}_\parallel^{(\gamma)}(ij)\rangle = 2$, only LS terms contribute.

Now, it it straightforward to write the formula for the low-energy spin-orbital Hamiltonian [18] which includes the superexchange terms due to e_g (H_J^e) and t_{2g} (H_J^t) charge excitations, the JT orbital interactions ($H_{\rm JT}$), and tetragonal crystal field (H_z),

$$\mathcal{H}_{\rm som} = H_J^e + H_J^t + H_{\rm JT} + H_z, \tag{7}$$

where

$$H_J^e = J\sum_{\langle ij\rangle\parallel\gamma}\left\{-\frac{1}{40}r_1(\vec{S}_i\cdot\vec{S}_j+6)\mathcal{Q}_\perp^{(\gamma)}(ij) + \frac{1}{320}(3r_2+5r_3)(\vec{S}_i\cdot\vec{S}_j-4)\mathcal{Q}_\perp^{(\gamma)}(ij) + \frac{1}{64}(r_4+r_5)(\vec{S}_i\cdot\vec{S}_j-4)\mathcal{Q}_\parallel^{(\gamma)}(ij)\right\} \tag{8}$$

and

$$H_J^t = \frac{1}{9}Jr_t\sum_{\langle ij\rangle}(\vec{S}_i\cdot\vec{S}_j-4). \tag{9}$$

The superexchange energy $J = 4t^2/U$ is here isotropic. The multiplet structure of e_g excited states is given by $\eta_e \equiv J_H^e/U$ which defines the coefficients,

$$r_1 = \frac{1}{1-3\eta_e}, \quad r_2 = \frac{1}{1+3\eta_e/4},$$
$$r_3 = r_4 = \frac{1}{1+5\eta_e/4}, \quad r_5 = \frac{1}{1+13\eta_e/4}. \tag{10}$$

TABLE I. Microscopic parameters of $LaMnO_3$ defining the spin-orbital cubic model of Ref. [18] (all in eV): effective ($dd\sigma$) hopping t, intraorbital Coulomb element U, Hund's exchange for e_g (J_H^e) and t_{2g} (J_H^t) electrons, and the orbital-orbital interaction induced by the JT effect κ (12).

t	U	J_H^e	J_H^t	κ
0.37	4.0	0.69	0.59	0.006

For t_{2g} charge excitations are given by $\eta_t \equiv J_H^t/U$ and it is convenient to introduce a single coefficient in Eq. (9) [18],

$$r_t = \frac{1}{8}\left(\frac{1}{4+5\eta_t} + \frac{1}{4+9\eta_t} + \frac{1}{4+11\eta_t} + \frac{1}{4+15\eta_t}\right). \tag{11}$$

The JT Hamiltonian $H_{\rm JT}$ describes the coupling between the adjacent sites via the mutual octahedron distortion. We note that the JT effect is connected with the oxygen atoms displacements which result in longer and shorter Mn-O bonds in ab planes but leave the manganese positions unchanged. The JT term is controlled by a single parameter $\kappa > 0$ that describes the rigidity of the oxygen positions (or the magnitude of displacement caused by the adjacent Mn orbital state). The effective orbital intersite interaction term is given by the orbital operators $\{\tau_i^{(\gamma)}\}$ as follows:

$$H_{\rm JT} = 8\kappa\sum_{\langle ij\rangle}\tau_i^{(\gamma)}\tau_j^{(\gamma)}. \tag{12}$$

This term favors AO order in the ab FM planes and dominates over the superexchange [24,30]. Finally, the last term in Eq. (7) stands for the tetragonal splitting of e_g orbitals and is introduced below in Sec. III. Both $H_{\rm JT}$ and H_z (see Sec. III A) modify the e_g superexchange via the orbital order at zero temperature ($T = 0$) [16].

In our previous paper [18] we investigated the consequences of the model of the $LaMnO_3$ crystal described in the literature, using the established parameters listed in Table I. The tetragonal splitting of e_g orbitals $\propto E_z$ was neglected. We performed mean field (MF) (cluster) calculations at finite temperatures. This allowed us to fit the values of parameters in the spin-orbital model, to make it the most reliable for the experimental situation. Our scrutiny revealed however, that even in that case, the model predictions are not fully consistent with the experiments (especially, when it comes to the value of the orbital mixing angle). We eliminated the possibility that the discrepancy may stem from the way we solved the model. (We showed that the short-range correlations play only a moderate role in this case and cannot break the MF-based methodology). This motivates us to make the model more realistic by going beyond the cubic symmetry.

B. Tetragonal geometry of $LaMnO_3$

In the $LaMnO_3$ crystal the manganese ions are arranged in a tetragonal lattice. In terms of the *Pmna* space group crystallographic axes a, b, and c, the Mn-Mn distances are given by $\frac{1}{2}\sqrt{a^2+b^2}$ in the FM ab planes and $c/2$ along the

AF c axis. The measured (at $T = 300$ K) values of these structural constants are [31]: $a = 5.5378$ Å, $b = 5.7385$ Å, and $c = 7.7024$ Å, so that the Mn-Mn distances are equal to 3.9874 Å in the ab planes and 3.8512 Å along the c axis. The relative difference in the lengths is as big as 3.5%.

To appreciate fully the consequences of tetragonal distortion, one has to include oxygen bridge positions in between neighboring manganese pairs which influence the electronic structure. The exact values of the corresponding Mn-O distances depend on: (i) the overall distance of two involved manganese ions and (ii) JT-like oxygens displacements. The JT effect is taken into account by a specially designed effective JT Hamiltonian Eq. (12) with $\kappa \simeq 6$ meV, see Table I, and there is no need to change it on the first instance. On the other hand, to assess the influence of the anisotropy of Mn-Mn distances, the cubic model has to be somehow extended.

As the oxygens JT-like displacements are described separately, the starting geometry for our tetragonal crystal model is established by putting the oxygen atoms directly halfway between the neighboring manganese ions. Thus the Mn-O bond lengths are set to 1.9937 and 1.9256 Å, respectively. In such a geometry there are deformed MnO_6 octahedra of D_{4h} point symmetry. In this work we will present the results for "rounded" values 1.995 Å (for the planar ab axes) and 1.925 Å (along the c axis). These values may be compared with the value for nondeformed MnO_6 octahedra with Mn-O distances equal to 1.970 Å.

C. Changes in comparison to the cubic model

We identify three main modifications that should be made to transform the well known cubic model [16] into a tetragonal model:

(i) The first change concerns the *tetragonal* CF effect itself. While displacements of oxygen atoms are well described by the JT Hamiltonian, the Mn-Mn distances influence the spin-orbital state by *tetragonal* CF. The *tetragonal* CF was introduced in Ref. [16] but its strength was not widely discussed.

(ii) The second change concerns the d-p hopping integral. In superexchange theory the virtual processes are perceived as a sequence of the electron's hoppings. The closer the involved atoms lie, the stronger the superexchange is. As far as we know, this effect has never been discussed.

(iii) The third change concerns the energies of charge excitations $\{\varepsilon_n\}$, given in Refs. [6,17]. In the superexchange theory excited virtual configurations are considered (for example the $^6A_1$ term for the HS d^5-d^3 excitation). The charge excitation energies depend on relative geometry (especially atom distances). In the tetragonal model the interatomic distances in one direction are different than the distances in the other two directions. Hence the corresponding energies in the model should be renormalized. As far as we know, this effect also has not been discussed earlier.

In this work we assess the importance of all the above changes. As necessary steps we evaluate the strength of the *tetragonal* CF and the change in the hopping integrals using remote quantum-chemical models.

III. TETRAGONAL CRYSTAL-FIELD SPLITTING

A. Definition of the crystal-field splitting

We investigated a generalization of the $LaMnO_3$ cubic model by introducing tetragonal CF. The *tetragonal* CF is modeled by the Hamiltonian H_z that is governed by a single parameter E_z, describing the energetic splitting of the e_g states (2):

$$H_z = \frac{1}{2}E_z \sum_i (|i\zeta_c\rangle\langle i\zeta_c| - |i\xi_c\rangle\langle i\xi_c|) = E_z \sum_i \tau_i^{(c)}. \quad (13)$$

For positive values ($E_z > 0$), $|\xi_c\rangle$ (i.e., $|x^2 - y^2\rangle$ states) are favored, whereas for negative values ($E_z < 0$), $|\zeta_c\rangle$ (i.e., $|3z^2 - r^2\rangle$) states have lower energy. For the realistic structure of $LaMnO_3$ one has $E_z > 0$. The bigger the value E_z is, the greater the contribution of $|x^2 - y^2\rangle$ orbitals is obtained (and the value of ϑ increases approaching 180°). If the *tetragonal* CF is ignored ($E_z = 0$) then the orbital mixing angle (at $T = 0$) is equal to 84° [6] contradicting the experiment; the experimental value $\vartheta_{\rm exp} = 108°$ [26] is reproduced in the model with $E_z \simeq 190$ meV (see the following section).

B. Impact of the CF splitting on spin-orbital order

We used on-site MF calculation scheme to determine the value of orbital mixing angle ϑ, *energy per site* E, and spin *exchange constants* J_γ ($\gamma = a,b,c$). The calculations revealed that the A-AF/C-AO state is destroyed by sufficiently strong tetragonal CF and the way the pattern decomposes under the influence of the tetragonal CF is quite nontrivial.

The spin A-AF pattern is obtained only when spin exchange constants fulfill $J_a = J_b < 0$ and $J_c > 0$. Their values depend on ϑ which, in turn, strongly depends on the actual CF splitting E_z (13). It turns out that the first constraint ($J_a = J_b < 0$) is not valid for $\vartheta > \vartheta^{\rm cr} \simeq 122°$ that occurs when the A-AF state breaks down at $E_z^{\rm cr} \simeq 291$ meV.

However, in reality, even when tetragonal CF is weaker than the critical value $E_z < E_z^{\rm cr}$, the A-AF state may not be the true ground state. Calculations reveal that even comparatively weak tetragonal CF may be strong enough to trigger spin reorientation. More precisely, when tetragonal CF is sufficiently strong, it is favorable for the spins to turn around and to change their order discontinuously from A-AF into G-AF. The transition is accompanied by a discontinuous jump of the *orbital mixing angle* (from ∼110° to ∼150°). The transition occurs for $E_z = E_z^{\rm cr} \simeq 188$ meV.

A physical explanation of the transition between different magnetic states is as follows: The A-AF state coexists with the orbital state characterized by $\vartheta_{(A\text{-AF})} \simeq 110°$, whereas G-AF state coexists with the orbital state characterized by $\vartheta_{(G\text{-AF})} \simeq 150°$. (Given values are for $E_z \simeq 200$ meV; of course $\vartheta \nearrow$ when $E_z \nearrow$ for the both cases but a key relation $\vartheta_{(G\text{-AF})} \gg \vartheta_{(A\text{-AF})}$ is valid for wide range of E_z.) In the absence of tetragonal CF, the A-AF state is the ground state. On the other hand, the tetragonal CF prefers states with larger angle ϑ. As one state is preferred when tetragonal CF is weak and the other is favored at strong tetragonal CF, the transition in between is rationalized.

The results of our calculations are summarized in Fig. 1. For the both types of spin order (A-AF and G-AF) their

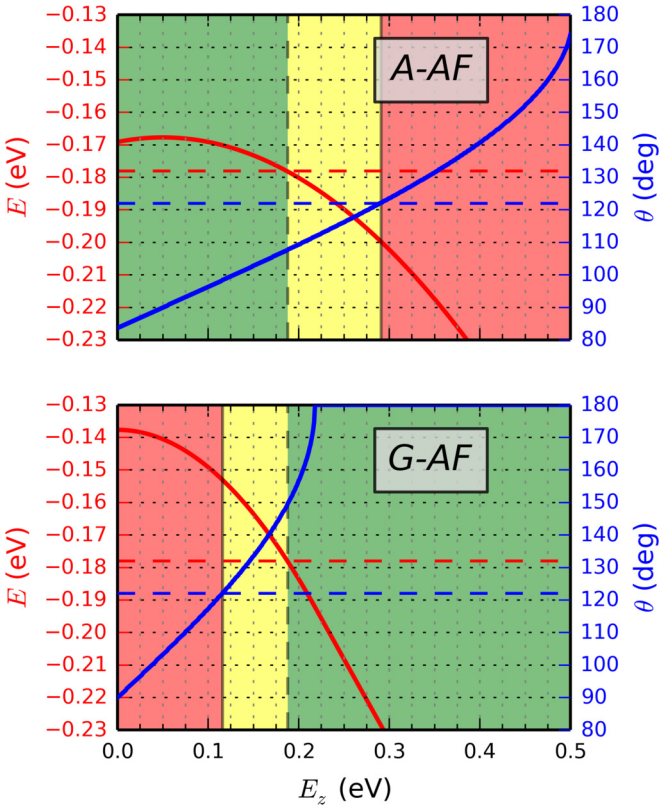

FIG. 1. Graphical representation of the influence of the tetragonal CF E_z (13) on the A-AF state (upper panel) and G-AF state (lower panel). Other parameters as in Table I. Background colors indicate the regimes of green: the ground state, yellow: a metastable excited state, and red: inconsistency for each type of spin order. Solid lines show the *energy per site* E (red) and the *orbital mixing angle* ϑ (blue). The horizontal dashed red line indicates the energy of the configurations at the quantum phase transition (at E_z^{QPT}), while the horizontal dashed blue line indicates ϑ^{cr}.

regimes of existence are indicated (background color different than red). Then, each such regime of existence is divided into two parts where the considered type of spin order is the ground state (green background color) and the excited state (yellow background color). In addition, for the both spin states *energy per site* E and *orbital mixing angle* ϑ are plotted (as a function of E_z).

It is important to mention that in an on-site MF calculation scheme a C-AO state and a G-AO state (both with the same spin order) give rise to solutions with identical energy per site E and orbital mixing angle ϑ. These states may be perceived as stacks of planes of the same type (namely antiferro-orbital planes). What differs the states is a relative displacement of the adjacent planes: the interplane bonds are either $|\pm\vartheta\rangle|\pm\vartheta\rangle$ (in C-AO phase) or $|\pm\vartheta\rangle|\mp\vartheta\rangle$ (in G-AO phase). The energy contributions from "in-plane bonds" (bonds $\langle ij\rangle\|ab$) are the same for both states (as they consist of the same planes) and do not differentiate the two states. Each energy contribution from the "interplane bond" (bond $\langle ij\rangle\|c$) depends on the orbital operators $\{\tau_i^{(c)},\tau_j^{(c)}\}$. However, exclusively for direction c: $\langle+\vartheta|\tau^{(c)}|+\vartheta\rangle = \langle-\vartheta|\tau^{(c)}|-\vartheta\rangle$, so that the prospective structural difference has no influence on the bonds energy contributions. As a result, the adjacent planes relative orientation does not matter for energy value. The results presented in this section are for C-AO and G-AO patterns; we have verified that solutions for ferro-orbital (FO) or A-AO patterns have higher energy.

TABLE II. The calculated values of tetragonal splitting E_z (in meV) in $LaMnO_3$ at different sophistication levels of the theory.

Number	Method	Basis set	Ext. charges	E_z
1	HF	STO-3G	✓	469
2	HF	6-31G	✓	309
3	HF	6-311G	✓	296
4	HF	6-311G*	✓	299
5	DFT (B3LYP)	STO-3G	✓	434
6	HF	STO-3G	absent	465

C. The value of tetragonal crystal-field splitting

The strength of the tetragonal CF splitting E_z (13) distinguishes between two HS states: $t_{2g}^3 z^1$ state and $t_{2g}^3 \bar{z}^1$ state. The splitting depends on the actual MnO_6 octahedron deformation (in other words, on Mn-O bond lengths). For calculations we take the reference geometry in which $\mathrm{Mn}-\mathrm{O}\|c$ axis bond length is equal to 1.925 Å and $\mathrm{Mn}-\mathrm{O}\|ab$ plane bond length is equal to 1.995 Å. The deformed octahedron anion $[\mathrm{Mn^{III}O_6}]^{9-}$ was used as a quantum chemical model. The anion was immersed in charge lattice that is to mimic the other ions that made up the crystal. The final values of E_z obtained in different quantum chemical levels of theory are shown in Table II.

At the beginning we carried out Hartree-Fock (HF) calculations in minimal basis set (STO-3G) in a given geometry and imposed multiplicity (quintet). We used a standard linear combination of an atomic orbitals (LCAO) scheme of unrestricted HF implementation (UHF). Each molecular HF calculation run was followed by the standard promolecule calculation that sets an initial-guess density matrix. As expected on grounds of ligand field theory, the obtained HF state's highest occupied molecular orbital (HOMO) is e_g^* molecular orbital (MO) with significant occupancy of the $\bar{z}$ atomic orbital (orbital symmetry B_{1g}) at manganese ions, whereas the lowest unoccupied MO (LUMO) is e_g^* MO with significant occupancy of the z^2 atomic orbital (orbital symmetry: A_{1g}). Hence, the obtained state corresponds to the model $t_{2g}^3\xi_c^1$ configuration.

Then, the second HF calculation was carried out. But in this case, the calculation started from a hand-made initial-guess density matrix determined from MOs obtained in the previous HF calculation run—the initial-guess configuration was a build of the LUMO and all occupied MOs but the HOMO. As in the course of HF iterations MOs was changed only quantitatively (not qualitatively), the obtained state was labeled as the model $t_{2g}^3 z^1$ configuration. A desired outcome of these calculations—the strength of tetragonal CF (parameter E_z)—was calculated as a difference between the energies of two obtained states. At the lowest level of the theory with the minimal basis set (STO-3G) one finds $E_z^{(1)} = 469$ meV.

It is a common wisdom that the calculations using the minimal basis set usually give a decent physical insight, but are not of sufficient quality and should be treated as pilot calculations only. Motivated by that we attempted to repeat

calculations using some bigger Popple basis sets. Unfortunately, the calculations were misleading. The first HF run ended up with converged HF (ground) state made of MOs that bear no resemblance to the standard ligand field theory like orbitals (e.g. e_g^* orbitals). Thus the obtained energies could not be used in the evaluation of E_z.

To overcome this problem we designed a modified calculation strategy for bigger basis sets. The modification applies to initial-guess states (implemented for both HF calculation runs: the one intended to describe $t_{2g}^3\bar{z}^1$ configuration and the other one for $t_{2g}^3 z^1$ configuration). The initial-guess states were calculated as projections of the corresponding states obtained in the minimal basis set calculations. The projections allow us to translate state description from one basis set to another basis set. (Of course the translated state is not strictly equivalent of the original state, but it is the closest possible match.) Then the typical HF convergence run was carried out. For 6-31G basis set calculations the HF iterations, fortunately, changed the initial guesses only quantitatively and we arrived at the proper solutions for this improved second level of the theory. The corresponding final result is $E_z^{(2)} = 309$ meV.

The convergence to the proper (ligand field theory like) solutions is a matter of luck. Typically HF iterations tend to change the nature of MOs so that calculations end in another physical solution. To avoid undesired configurations one may rely on imposing the symmetry types of occupied MOs. In our case it would imply imposing the total numbers of B_{1g}-type occupied MOs and the total number of A_{1g}-type occupied MOs. However, typical implementations of this trick applies for a maximal Abelian symmetry subgroup (as they have solely nondegenerate irreducible representations that are easy to handle). Deformed MnO_6 octahedron has D_{4h} symmetry, with a maximal Abelian subgroup D_{2h}. In terms of the D_{2h} group the x^2-y^2-like orbitals and z^2-like orbitals have the same symmetry, i.e., A_g (there are no B type representations in the D_{2h} group). This rules out the possibility of applying the above trick in our study.

We repeated the modified procedure to obtain the results for bigger and bigger basis sets. We were changing the basis gradually, see the calculation numbers 1–4 in Table II. States were projected many times, so that every HF run (except for the minimal basis set calculations) started with a projected state obtained in only a slightly smaller basis calculation. The numeric values of E_z for a larger than minimal basis set do not differ significantly so no further correction is needed to predict a limiting value for an infinite basis,

$$E_z^{\mathrm{HF}} \simeq 300 \text{ meV}. \tag{14}$$

To verify this prediction we compared the obtained HF results in Table II for the minimal basis set STO-3G (number 1) with the corresponding calculations in DFT theory (we used the popular B3LYP functional [32,33]), see number 5, to check whether the electron correlation effects may be significant in our problem. The comparison reveals that HF (number 1) tends to overestimate the value of E_z for about 7%. Eventually, we verified that, to our surprise, the external charges in the lattice have a negligible effect, see number 6 in Table II.

Altogether we confirm that $E_z > 0$ in $LaMnO_3$ in the low temperature phase with tetragonal distortion. However, our calculations suggest a value in Eq. (14) which is about twice larger than that determined before by Flesch *et al.* [24].

IV. REVISED SUPEREXCHANGE MODEL

A. The origin of the superexchange Hamiltonian

Integrating out the high-energy intermediate states obtained by charge excitations gives rise to the effective low-energy interactions; each excitation contributes to a spin-orbital superexchange Hamiltonian (which we use). In this way energies of the excited charge configurations appear in the effective Hamiltonian and define its parameters.

Both Mott insulators and CT insulators are described in terms of superexchange when electron correlations are strong. In both cases the sets of contributing virtual processes are the same, however their relative importance depends on the actual parameters which control these processes. In general, the sequence of four hopping processes appears along an M-O-M bond,

$$\begin{aligned} M^m L^n M^m &\xrightarrow{(1)} M^{m+1} L^{n-1} M^m \\ &\xrightarrow{(2)} M^{m+1} L^n M^{m-1} \\ &\xrightarrow{(3)} M^{m+1} L^{n-1} M^m \\ &\xrightarrow{(4)} M^m L^n M^m \end{aligned} \tag{15}$$

and describes leading processes for Mott insulators (in a term $M^{m_1} L^{n_1} M^{m_2}$ the leftmost M-ion electron shell corresponds on one magnetic cation, the L orbital shell in between (of an O ion) belongs to the bridge ligand, and the rightmost M-ion electron shell is localized on the neighboring magnetic cation). These processes involve a hopping integral t_{pd} between the $\mathrm{Mn}(3d_{z^2})$ orbital and the bridge oxygen $\mathrm{O}(2p_z)$ orbital for a bond along the bond in each step.

In particular cases the electronic configurations of intermediate states are realized by various atomic terms. For example, in case of a simple "toy model" of a Mott insulator for metals and ligands with only a single interacting orbital, the structure of terms is trivial and the low-energy Hamiltonian reads [34]

$$H_{\langle ij\rangle} = \frac{4t_{pd}^4}{\Delta^2}\left(\frac{1}{U_d} + \frac{2}{2\Delta + U_p}\right)\vec{S}_i \cdot \vec{S}_j \simeq \frac{4t_{pd}^4}{\Delta^2 U}\vec{S}_i \cdot \vec{S}_j, \tag{16}$$

with U_d (U_p) being the intraorbital Coulomb elements for $3d$ ($2p$) orbitals, ϵ_d (ϵ_p) being the electron energy in orbital $3d$ ($2p$), and the charge transfer (CT) excitation energy is

$$\Delta \equiv U_d - U_p + \epsilon_d - \epsilon_p. \tag{17}$$

The first (second) term in Eq. (16) is called the Anderson (Goodenough) contribution, both defined by the nature of charge excitations, either an M or an O ion. Here we introduced an effective Coulomb element U to describe the superexchange by the Anderson process. Note that $U \simeq U_d$ for Mott insulators, with $\Delta \gg U_d$, while otherwise $U \simeq \Delta$.

Although the manganite case is much more involved than the toy model, the general patterns of superexchange terms are similar in both cases. In the case of the $LaMnO_3$ crystal the values U_d and Δ in Eq. (16) correspond to excitation energies to

$(3d)^5(2p)^6(3d)^3$ and $(3d)^5(2p)^5(3d)^4$ configurations. Hence, a general bond term in the superexchange Hamiltonian is proportional to

$$\left(\frac{t_{pd}^2}{E[(3d)^5(2p)^5(3d)^4]}\right)^2 \frac{1}{E[(3d)^5(2p)^6(3d)^3]} \times \begin{pmatrix}\text{certain spin}\\ \text{operator}\end{pmatrix} \times \begin{pmatrix}\text{orbital projection}\\ \text{operator}\end{pmatrix}. \quad (18)$$

The expression in the first bracket describes the effective Mn-Mn hopping

$$t_\gamma \equiv \frac{t_{pd}^2(d_\gamma)}{E[(3d)^5(2p)^5(3d)^4]}, \quad (19)$$

in the effective model $\mathcal{H}_{\text{som}}$ (in which oxygen ions are absent). Here $t_{pd}(d_\gamma)$ is the hybridization element for the Mn-O bond of length d_γ. The exact form of the Hamiltonian was derived in Ref. [16]. Our key observation is that the parameters in Eq. (18) depend on crystal geometry. Moreover, the directional renormalization of t_{pd} is amplified by a factor of 4 in superexchange which results from processes of the type $\propto t_\gamma^2/U$ in perturbation theory. In the two following subsections we analyze separately the dependence on geometry of (i) $t_{pd}(d_\gamma)$ and (ii) the energies of the excited state.

B. Renormalization of t_{pd}

We tried to assess the relative change of the value of hopping integral t_{pd} that follows from the Mn-O-Mn bonds length change. Once more we built a quantum chemical model that serves to describe the localized orbitals in the crystal. We believe that it is sufficiently accurate to investigate the relative change in t_{pd} value.

It is quite nontrivial to assign concrete orbitals that correspond to "metal $3d_{z^2}$ orbital" and "oxygen $2p_z$ orbital"—the basis orbitals in terms of elementary (not effective) superexchange models (with metal and oxygen ions treated individually). It is a fundamental assumption in these models that the orbitals are orthogonal. It rules out the possibility of direct usage of the corresponding atomic orbitals. It is a temptation to use MOs instead (similar to that described in a previous section). However this approach is also not valid. In terms of the elementary superexchange model, for which t_{pd} is a parameter, the MOs are linear combinations of the basis orbitals—the results of coupling the basis orbitals mediated by t_{pd} (being an off-diagonal Hamiltonian matrix element).

Here we propose to start with atomic orbitals (using STO-6G) and take advantage of an orthogonalization scheme that minimizes the orbital changes, namely the Löwdin orthogonalization. In this way we obtain a pair of the orthogonal adjacent Löwdin orbitals: the metal $3d_{z^2}$-like orbital (labeled "e_g^*") and the oxygen $2p_z$-like orbital (labeled "$\perp e_g^*$") of the form that is shown in Fig. 2.

Superexchange models introduce simple and intuitive descriptions in which only a few electrons are treated explicitly, whereas the majority of all remaining electrons (those occupying inner shells and some outer shells) are treated implicitly. The latter are assumed to be fixed and, together with nuclei, build up a specific scene in which the explicitly treated electrons are immersed. In our case atoms configurations made

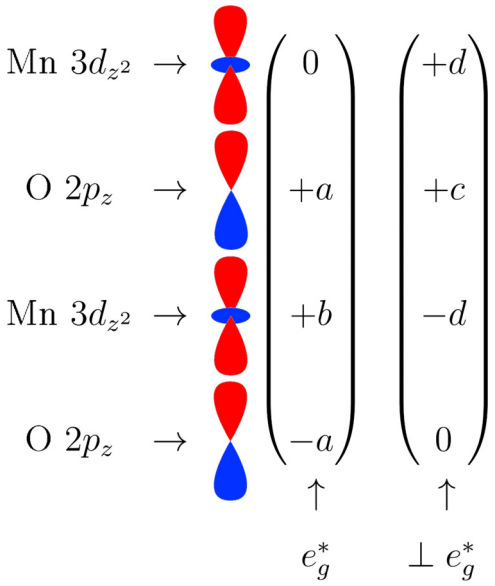

FIG. 2. The general form of basis MOs used to derive the superexchange model. The values of t_{pd} depend on the overlap between the adjacent atomic orbitals. The parameters b and c are close to unity for the orbitals centered at Mn and O ions along the c axis, whereas the values of a and d are close to zero (as long as electrons localize and the overlap is small).

up by the implicitly treated electrons read

$$\text{Mn}^{4+} : [\text{Ar}](3t_{2g})^3, \text{O}(\gamma) : [\text{He}](2s)^2(2p_{\perp\gamma})^4, \text{La}^{3+} : [\text{Rd}],$$

where $\text{O}(\gamma)$ denotes the oxygen atoms belonging to the Mn-O-Mn bridges parallel to γ direction and $2p_{\perp\gamma}$ denotes pairs of $2p$ orbitals perpendicular to γ direction. We will use Löwdin orbitals (STO-6G) as a specific realization of the abstract orbitals included in the above configuration scheme. This allows us to use standard MF approximation to introduce interactions with the given implicitly treated electrons.

The t_{pd} is a one-electron mean field Hamiltonian off-diagonal matrix element. In terms introduced above one finds

$$t_{pd} = \langle e_g^* | H_{1e}^{\text{MF}} | \perp e_g^* \rangle, \quad (20)$$

where

$$\hat{H}_{1e}^{\text{MF}} = \hat{T} + \hat{V}_{en} + \hat{J} + \hat{K} \quad (21)$$

encompasses a single electron kinetic energy ($\hat{T}$), electron-nuclei Coulomb interaction ($\hat{V}_{en}$), electron-electron Coulomb interaction with the implicitly treated electrons that gives rise to Coulomb ($\hat{J}$), and exchange contribution ($\hat{K}$). The Coulomb contribution bears a resemblance to the classical Coulomb interaction between an electron and the mean electrostatic charge distribution of the implicitly electrons. In contrast, exchange contribution is purely quantum. The form of the Hamiltonian in Eq. (21) is analogous to the MF one-electron Hamiltonian used in the Hartree-Fock method.

Having the concrete form of the orbitals and after identifying the implicitly treated electrons, we were able to evaluate the value of t_{pd} according to Eq. (20). We constructed the cluster of many unit cells to mimic the crystal environment.

TABLE III. The directional renormalization factors for the hybridization elements t_{pd}, the effective $(dd\sigma)$ hopping t_γ which depends on bond direction γ, the energies of final states for charge transfer excitation Δ, and for interionic Mn-Mn charge excitations ε_n with $n = 1, \ldots, 4$.

Energy	Excited state		Bond renormalization	
	Mn-O-Mn		$\langle ij\rangle \| a(b)$	$\langle ij\rangle \| c$
t_{pd}			94.8%	111.5%
t_γ			90.3%	123.7%
	Mn-O excitation	$(3d)^5$		
Δ	$(3d)^5(2p)^5(3d)^4$	$^4A_1$	99.5%	100.5%
	Mn-Mn excitation			
ε_1	$(3d)^5(2p)^6(3d)^3$	$^6A_1$	102.3%	95.6%
ε_2	$(3d)^5(2p)^6(3d)^3$	$^4A_1$	101.0%	98.1%
ε_3	$(3d)^5(2p)^6(3d)^3$	^4E	100.9%	98.3%
ε_4	$(3d)^5(2p)^6(3d)^3$	$^4A_2$	100.7%	98.6%

Then, we invoked the approximation in which all implicitly treated electrons localized at atoms different than the hopping spots are treated as classical point charges (unit minus charges localized on the atomic centers). The obtained results for the actual bond lengths in the ab planes and along the c axis are (in eV)

$$t_{pd}(1.995\ \text{Å}) = 2.00, \quad t_{pd}(1.925\ \text{Å}) = 2.35. \tag{22}$$

These changes are in excellent agreement with the semiempirical law of Harrison which gives $t_{pd} \propto d_\gamma^{-4}$ for a Mn-O bond of length d_γ [35]. For a shorter bond along the c axis of 97.72%, one finds the increase of t_{pd} to 109.7%, while the Harrison's law gives 111.4%. For a bond longer by 101.27% in the ab plane one finds t_{pd} decreased to 94.8%, while the Harrison's law predicts 95.1%. Indeed, these results verify the semiempirical Harrison's law and one finds a significant difference in the t_{pd} values (22). A kinetic energy contribution is roughly equal to 5.0 eV and an electrostatic potential contribution is roughly equal to -3.0 eV (it includes the repulsive interaction with core electrons). In addition to this we found a weak (-0.3 eV) exchange contribution. We compare these values with the value obtained for the cubic geometry (2.11 eV) to get the t_{pd} renormalization factors that should be imposed when changing the cubic model into a tetragonal one, the first row in Table III.

Due to the large difference in the values of t_{pd}, the effective hopping elements t_{ab} and t_c for the bonds $\|ab$ and $\|c$, respectively, exhibit remarkably large anisotropy and $t_c/t_{ab} = 1.37$, see Table III. This large difference may be obtained under neglect of the small anisotropy of CT excitations, see the next section, and modifies even more the anisotropic e_g exchange interactions due to their quadratic dependence on the hopping $J_\gamma^e \propto 4t_\gamma^2/U$, and thus influences the spin-orbital order.

C. Renormalization of the excitation energies

In the superexchange approach all the virtual excited states are CT states (in the sense that there is a surplus positive charge located in one lattice node accompanied by a surplus negative charge located in another lattice node). Energy of a CT configuration may be roughly divided into three parts: the first part describes ionization energy of the first CT state moiety, the second part describes electron affinity of the second CT state moiety, and the third part describes an internal Coulomb interaction between the surplus charges as well as their Coulomb interaction with a surrounding charge distribution. The first two parts are CT intermoiety separation independent. On the other hand, the third part is directly a crystal geometry dependent part. For example, the Coulomb interaction between the surplus charges is inversely proportional to intermoiety distance (from the simplest and approximate point of view).

Let us consider one of the virtual CT states: $(3d)^5(2p)^6(3d)^3$. In this state the surplus unit negative charge is localized on the first Mn atom and the surplus unit positive charge is localized on the second Mn atom (in other words, it is the configuration Mn^{2+}-Mn^{4+}). For Mn ions the $(3d)^5$ configuration may be realized by four electronic terms: $^6A_1$, $^4A_1$, ^4E, and $^4A_2$, with the excitation energies [17] 1.93, 4.52, 4.86, and 6.24 eV, using the parameters of Table I. In the reference cubic geometry Mn-Mn distance is equal to 3.94 Å and the Coulomb interaction energy between surplus charges is equal to -3.655 eV. In the tetragonal geometry, in which in one crystallographic direction Mn-Mn distances are equal to 3.99 or 3.85 Å, and the corresponding Coulomb interaction energy is -3.609 or -3.740 eV, respectively.

In addition to this, the surplus charges surrounding ion interactions should be considered; however in this case they cancel out as the surplus charges are located on the equivalent lattice positions. It means that the contribution to total excitation energy is bigger for 0.045 eV (or less for -0.085 eV). For example, for $^6A_1$ excitation this change gives rise to the renormalization of the total excitation energy by the factor 102.4% (or 95.6%). The renormalization results are collected in Table III.

Finally, there is as well the $(3d)^5(2p)^5(3d)^4$ configuration standing for a CT excitation. Its overall excitation energy is equal to 5.5 eV [36]. The corresponding electrostatic calculation is more involved in this case: as the opposite surplus charges are not located at equivalent lattice positions, one has to add surplus charges surrounding ion interactions energy. The surplus positive charge (located on an oxygen anion) has bigger energy if the hopping goes in the shortened direction. This effect is almost exactly compensated by the energy gain due to surplus charge stabilization (that appears if they are closer). The net result is that the excitation energies are barely split and the corresponding excitation energies renormalization factor is close to unity.

V. THE TETRAGONAL MODEL AT $T = 0$

A. Orbital mixing angle and exchange constants

The predictions of the tetragonal model Eq. (7) were investigated using on-site MF approximation and compared to the results obtained for the cubic model. We decided to implement the extensions accounting for tetragonal CF together with the directional renormalization of a hopping integral and neglect the weaker electrostatic effects. We focus in this section on the results obtained at $T = 0$. When temperature increases, the tetragonal deformation varies with T and a purely electronic model cannot be applied, see the Appendix.

The model parameter values were fitted to reproduce the available experimental observations. We used an effective hopping integral $t = t_{pd}^2/\Delta = 0.5$ eV (for CT energy $\Delta = 5.5$ eV [36] this corresponds to $t_{pd} = 1.66$ eV, reasonably close to the value 1.5 eV used before [16]). The temperature of the structural transition T_{OO} is only a fraction of the orbital exchange interaction [37] and alone would not explain the high value of T_{OO} [16,21–23]. Thus we included the JT effective parameter κ which was chosen at 4 meV (this value is lower than that used before [18] as a consequence of the increased values of the hopping parameters t_γ and enhanced superexchange). At the end we used $E_z = 300$ meV, in line with our external quantum chemical calculations (14), see Sec. III. Other physical parameters were the same as deduced for the cubic model, see Table I.

The obtained results are remarkably satisfactory—they reproduce all experimental data with reasonable accuracy. The orbital mixing angle ϑ (1) found for the tetragonal structure is equal to 106° and stays within excellent agreement with the experimental value 108°. This agreement could be achieved mainly due to finite tetragonal e_g orbital splitting. The estimated value $E_z = 300$ meV (14) fits perfectly.

Also the predicted values of the spin exchange constants $J_{ab} = -1.7$ meV and $J_c = +0.8$ meV (both at $T = 0$) are reasonably close to the experimental values -1.7 and 1.2 meV [38]. The results depend strongly on the introduced renormalization of the t_{pd} hopping integral (22) that gives rise to immense J_{ab} and J_c renormalization factors (-29% and 51%, respectively). Without them the $|J_{ab}|/J_c$ ratio would be incorrect. Although the values fit reasonably well, they are numerically uncertain as they are an algebraic sum of a few big (up to 9 meV) contributions of opposite sign. (The spin exchange constants consist of a strong FM superexchange term for the lowest energy $^6A_1$ excitation and several smaller AF terms.)

B. Discussion

As one may expect that the tetragonal crystal field E_z (13) is the most important correction to introduce, we tentatively investigated it at first as if it was the only needed correction (and neglected the other two proposed later). Within this approach, the discussed model was essentially the same as in Ref. [16]. At this stage we adopted, as a reference starting point, the cubic model parameter values from our earlier work [18] that was devoted to the (implicitly) cubic model. The phase diagram was examined against the e_g orbital splitting, i.e., tetragonal crystal field E_z, see Fig. 1. We have found that a too strong crystal field (greater than 0.2 eV) could have destabilized the observed A-AF state. This transition bears great resemblance to the transition between A-AF phase and G-AFx phase described in Ref. [16]. The only difference is that the G-AF phase with adjusted orbitals arises in addition between the two phases (for very tiny range of E_z).

Next the dependence between orbital mixing angle and the tetragonal crystal field magnitude was plotted. As expected, the tetragonal crystal field enhances the amplitude of the $|x^2 - y^2\rangle$ orbital state (the $|3z^2 - r^2\rangle$ counterpart contributes mainly to excited states at both sublattices). We carried out independent quantum chemical calculations to evaluate the value of $E_z = 300$ meV (14) and an enhanced value of $t = 0.5$ eV instead of $t = 0.37$ eV, see Table I. We conclude that the entire picture is consistent (and more realistic than the one offered by the implicitly cubic model). Thus we suggest that it may be used as a starting point to include finer corrections (considering directional renormalization).

Then, to establish an even more reliable Hamiltonian, we investigated the origin of superexchange terms. Improvements include the directional dependence of the hopping integral t_{pd} values as well as the excitation energies of virtual charge excited states. The directional deviations of the values introduce directional renormalization factors of Hamiltonian terms that extend the cubic Hamiltonian analyzed earlier. We employed chemical models to evaluate the renormalization factors in an approximate way using first-principle methods. The raw, classical calculations suggest that the changes of excitations energies are small — only up to a few percent — and may be neglected on the presented qualitative level of theory.

On the other hand, the anisotropy of hopping integrals (22) in the tetragonal structure is considerable. We found the following t_{pd} values: 2.11 eV for the cubic geometry and $t_{pd} \simeq 2.0$ eV or $t_{pd} \simeq 2.35$ eV for tetragonal geometry (depending on the bond direction), see Eqs. (22). The anisotropy of t_{pd} is enhanced by a factor of 2 in the Mn-Mn effective hopping, see Eq. (19). Note that the values of t_{pd} are here somewhat larger than those used earlier (1.5 eV in Ref. [16]). The increase of t_{pd} may be rationalized by the fact that Mn-O bonds in our conceived tetragonal model are shorter than in the real crystal (the Mn-O-Mn bridges bend as described in the first paragraph of this section). For the real Mn-O bond lengths, obtained t_{pd} values would be smaller.

VI. SUMMARY

In this work we analyzed diverse physical aspects that emerge due to the nonequivalence of all three crystallographic directions in the experimental crystal structure of $LaMnO_3$. In order to make the analysis conclusive the conceived tetragonal $LaMnO_3$ crystal model was introduced and investigated. We demonstrated that it offers a better overall description of the ground state in comparison with the cubic model used earlier. Despite apparent improvements, the introduced model adopts complicated structural effects only partially. In fact, the real $LaMnO_3$ crystal is nontetragonal due to additional MnO_6-octahedra tilts. The bridging oxygen atoms do not lie precisely on the line segments spanning the bridged manganese ion pairs—the oxygen atoms are translated aside the segments. The Mn-O-Mn bridges bend so that the Mn-O bonds are less strained. We believe that the corrections to the crystal electronic structure that stem from the tilts are of less importance and their qualitative description goes beyond the scope of this work.

Further support for the tetragonal model introduced here follows from its comparison with experiment, both at $T = 0$ and at finite temperature. The predicted electronic ground state was investigated in terms of the observables that may be compared with experiment: the spin exchange constants and the orbital mixing angle. We found excellent agreement with the experimental data when the Coulomb interaction parameters of Table I are used, but we had to adopt $t = 0.5$ eV and $\kappa = 4$ meV. This agreement certainly appears very encouraging as both the orbital angle and the exchange constants are well reproduced, in contrast to the earlier studies

[6,18]. Indeed, such a satisfactory scenario could not be obtained without the described directional renormalizations of t_{pd} which directly influence the J_c/J_{ab} ratio. At finite temperature we established a tentative link between structural deformation and the orbital order parameter. Using the tetragonal model Hamiltonian we predicted temperatures of spin (magnetic) and orbital phase transitions, see the Appendix. We observe no changes of transition temperatures due to the directional corrections, however the critical exponent for the orbital phase transition is modified as the tetragonal distortion is reduced together with orbital order.

Summarizing, we established the tetragonal model of $LaMnO_3$ by evaluating the corrections necessary to improve the model (7) derived initially for the perovskite structure. We conclude that for $LaMnO_3$ at least two physical effects connected with the inequality of Mn-O-Mn bridge distances are important and have to be included when carrying out quantitative calculations: (i) the tetragonal crystal field E_z (14) and (ii) direction-dependent renormalization of p-d hybridization t_{pd} (22). The first one is necessary to obtain the experimentally observed form of the occupied e_g orbitals in the ground state, i.e., the correct value of the orbital mixing angle (1) for the occupied states. The second one is responsible for the anisotropy of the dominating e_g part of superexchange and is crucial to reproduce the observed ratio of spin exchange constants J_c/J_{ab}. These effects are far stronger than the systematic corrections beyond the simplest on-site mean field described in our previous work [18]. We suggest that similar modifications of the ground state may be found in other correlated insulators when the present procedure was repeated for realistic crystal structure of similar transition metal compounds, for instance for $KCuF_3$ (although some technical problems could occur).

ACKNOWLEDGMENTS

We thank K. Rościszewski for insightful discussions. We kindly acknowledge support by Narodowe Centrum Nauki (NCN, National Science Centre, Poland) under Project No. 2016/23/B/ST3/00839.

APPENDIX: TETRAGONAL MODEL AT FINITE TEMPERATURE

The influence of renormalized parameters on (spin and orbital) transition temperatures is of particular interest. To analyze transition temperatures, on-site MF calculations were performed at finite temperature. We emphasize that as temperature increases the tetragonal deformation decreases, and starting from the orbital transition temperature T_{OO} the orbital order disappears [39] and the cubic model is valid again. Therefore the thermal dependence of deformation magnitude has to be included when performing on-site MF calculations at finite temperature.

The proposed model (7) is purely electronic and the structural deformation magnitude is one of its external parameters. The values of all the parameters, as well as their temperature dependence, have to be introduced as input. However, it is misleading to simply use a fixed function of temperature that describes the deformation, as the electronic state and crystal geometry are strictly interrelated. For instance, the calculations have to respect the physical requirement that the orbital order phase transition and structural phase transition take place simultaneously. To assure the consistency (between electronic and structural degrees of freedom) we use a strategy of dynamical updating of deformation magnitude as a function of electronic state. Although there is no direct way to gain information about the unit cell parameters from an electronic state we propose to do it straightforwardly. We postulate that the deformation is proportional to the on-site orbital order parameter $r(T)$. Hence we arrive at the heuristic equations:

$$E_z(T) = r(T)E_z(0), \tag{A1}$$

$$t_{pd,\gamma}(d_\gamma,T) = t_{pd}^{\square} + r(T)[t_{pd,\gamma}(d_\gamma,0) - t_{pd}^{\square}], \tag{A2}$$

where $t_{pd}^{\square}$ denotes the reference value for a cubic crystal. Our strategy may be verified *a posteriori* by a comparison of the obtained functional dependence of crystal deformation with available crystallographic data.

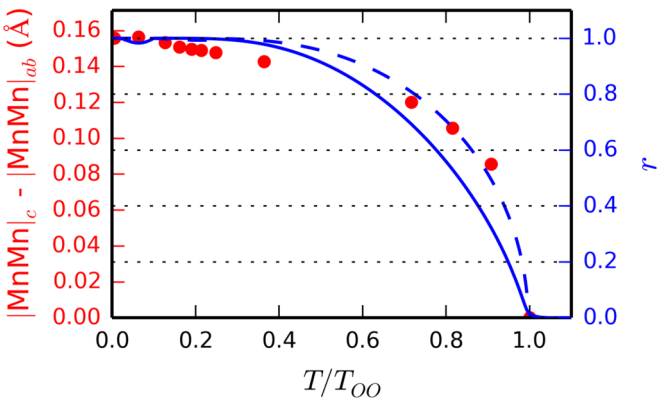

FIG. 3. Comparison of thermal dependencies of calculated orbital order parameter $r(T)$ (blue solid curve for tetragonal model and blue dashed curve for cubic model) with experimental data of tetragonal deformation magnitude (red points). The experimental data are from Ref. [26].

The tetragonal model gives in mean field approximation the following transition temperatures: 160 K for the magnetic transition and 1615 K for the simultaneous orbital/structural transition. As the experimental values are equal to 140 and 750 K the theory overestimates them by 115% and 215%. Indeed, one may expect enormous overestimation due to crude on-site MF approximation, and the overestimation factors up to 200% for the orbital pseudospin $\tau = 1/2$ are acceptable.

Finally, the heuristic assumption about the form of the interrelation between the electronic state and the structural deformation magnitude should be checked. We compare the shape of the temperature dependence of the measured deformation magnitude and the orbital order parameter $r(T)$ extracted from the theory. In order to compare the shape, both functions are expressed in terms of the reduced temperature T/T_{OO}, where T_{OO} is the corresponding orbital transition temperature (obtained within the present theory), see Fig. 3. Both curves are qualitatively similar and the agreement is fair.

The curve calculated for the tetragonal model fits better than the one for the cubic model in the low-to-intermediate temperature sector as it bends much stronger for $0.3 < T/T_{OO} < 0.7$. However, the curve for the cubic model offers a better approximation for the critical exponent

β. This seems to be a consequence of the temperature dependence of tetragonal distortion which modifies the orbital transition. We also note that remarkably fast decrease of the tetragonal deformation for $T/T_{OO} < 0.4$ cannot be reproduced in the electronic model—it may be expected that acoustic phonons are of importance in this regime and the deformation decreases faster than predicted in mean field theory. This question remains open for future studies.

[1] M. Imada, A. Fujimori, and Y. Tokura, Metal-insulator transitions, Rev. Mod. Phys. **70**, 1039 (1998).

[2] K. I. Kugel and D. I. Khomskii, The Jahn-Teller effect and magnetism: Transition metal compounds, Usp. Fiz. Nauk **136**, 621 (1982) [Sov. Phys. Usp. **25**, 231 (1982)].

[3] A. J. Millis, Cooperative Jahn-Teller effect and electron-phonon coupling in $La_{1-x}A_xMnO_3$, Phys. Rev. B **53**, 8434 (1996).

[4] I. Leonov, D. Korotin, N. Binggeli, V. I. Anisimov, and D. Vollhardt, Computation of correlation-induced atomic displacements and structural transformations in paramagnetic $KCuF_3$ and $LaMnO_3$, Phys. Rev. B **81**, 075109 (2010).

[5] G. Khaliullin, Orbital order and fluctuations in Mott insulator, Prog. Theor. Phys. Suppl. **160**, 155 (2005).

[6] A. M. Oleś, G. Khaliullin, P. Horsch, and L. F. Feiner, Fingerprints of spin-orbital physics in cubic Mott insulators: Magnetic exchange interactions and optical spectral weights, Phys. Rev. B **72**, 214431 (2005).

[7] A. Reitsma, L. F. Feiner, and A. M. Oleś, Orbital and spin physics in $LiNiO_2$ and $NaNiO_2$, New J. Phys. **7**, 121 (2005).

[8] A. Smerald and F. Mila, Disorder-Driven Spin-Orbital Liquid Behavior in the $Ba_3XSb_2O_9$ Materials, Phys. Rev. Lett. **115**, 147202 (2015); Exploring the spin-orbital ground state of $Ba_3XSb_2O_9$, Phys. Rev. B **90**, 094422 (2014).

[9] P. Corboz, M. Lajkó, A. M. Laüchli, K. Penc, and F. Mila, Spin-Orbital Quantum Liquid on the Honeycomb Lattice, Phys. Rev. X **2**, 041013 (2012).

[10] W. Brzezicki, A. M. Oleś, and M. Cuoco, Spin-Orbital Order Modified by Orbital Dilution in Transition-Metal Oxides: From Spin Defects to Frustrated Spins Polarizing Host Orbitals, Phys. Rev. X **5**, 011037 (2015).

[11] W. Brzezicki, M. Cuoco, and A. M. Oleś, Novel spin-orbital phases induced by orbital dilution, J. Supercond. Novel Magn. **29**, 563 (2016); Exotic spin-orbital physics in hybrid oxides, **30**, 129 (2017); W. Brzezicki, M. Cuoco, F. Forte, and A. M. Oleś, Topological phases emerging from spin-orbital physics, *ibid.* **31**, 639 (2018).

[12] E. Dagotto, T. Hotta, and A. Moreo, Colossal magnetoresistant materials: The key role of phase separation, Phys. Rep. **344**, 1 (2001); E. Dagotto, Open questions in CMR manganites, relevance of clustered states and analogies with other compounds including the cuprates, New J. Phys. **7**, 67 (2005).

[13] Y. Tokura, Critical features of colossal magnetoresistive manganites, Rep. Prog. Phys. **69**, 797 (2006).

[14] J. B. Grant and A. K. McMahan, Spin bags and quasiparticles in doped La_2CuO_4, Phys. Rev. B **46**, 8440 (1992).

[15] R. E. Walstedt and S.-W. Cheong, Covalency in La_2CuO_4: A study of ^{17}O hyperfine couplings in the paramagnetic phase, Phys. Rev. B **64**, 014404 (2001).

[16] L. F. Feiner and A. M. Oleś, Electronic origin of magnetic and orbital ordering in insulating $LaMnO_3$, Phys. Rev. B **59**, 3295 (1999).

[17] N. N. Kovaleva, A. M. Oleś, A. M. Balbashov, A. Maljuk, D. N. Argyriou, G. Khaliullin, and B. Keimer, Low-energy Mott-Hubbard excitations in $LaMnO_3$ probed by optical ellipsometry, Phys. Rev. B **81**, 235130 (2010).

[18] M. Snamina and A. M. Oleś, Spin-orbital order in the undoped manganite $LaMnO_3$ at finite temperature, Phys. Rev. B **94**, 214426 (2016).

[19] A. M. Oleś, Fingerprints of spin-orbital entanglement in transition metal oxides, J. Phys.: Condens. Matter **24**, 313201 (2012); Frustration and entanglement in compass and spin-orbital models, Acta Phys. Pol. A **127**, 163 (2015).

[20] W. Brzezicki, J. Dziarmaga, and A. M. Oleś, Noncollinear Magnetic Order Stabilized by Entangled Spin-Orbital Fluctuations, Phys. Rev. Lett. **109**, 237201 (2012); Exotic spin orders driven by orbital fluctuations in the Kugel-Khomskii model, Phys. Rev. B **87**, 064407 (2013); Topological Order in an Entangled Spin-Orbital SU(2)$\otimes XY$ Ring, Phys. Rev. Lett. **112**, 117204 (2014).

[21] D. Feinberg, P. Germain, M. Grilli, and G. Seibold, Joint superexchange-Jahn-Teller mechanism for layered antiferromagnetism in $LaMnO_3$, Phys. Rev. B **57**, R5583 (1998).

[22] S. Okamoto, S. Ishihara, and S. Maekawa, Orbital ordering in $LaMnO_3$: Electron-electron and electron-lattice interactions, Phys. Rev. B **65**, 144403 (2002).

[23] E. Pavarini and E. Koch, Origin of Jahn-Teller Distortion and Orbital Order in $LaMnO_3$, Phys. Rev. Lett. **104**, 086402 (2010).

[24] A. Flesch, G. Zhang, E. Koch, and E. Pavarini, Orbital-order melting in rare-earth manganites: Role of superexchange, Phys. Rev. B **85**, 035124 (2012).

[25] H. Sawada, Y. Morikawa, K. Terakura, and N. Hamada, Jahn-Teller distortion and magnetic structures in $LaMnO_3$, Phys. Rev. B **56**, 12154 (1997).

[26] J. Rodríguez-Carvajal, M. Hennion, F. Moussa, A. H. Moudden, L. Pinsard, and A. Revcolevschi, Neutron-diffraction study of the Jahn-Teller transition in stoichiometric $LaMnO_3$, Phys. Rev. B **57**, R3189 (1998).

[27] T. Mizokawa, D. I. Khomskii, and G. A. Sawatzky, Interplay between orbital ordering and lattice distortions in YVO_3, $YTiO_3$, and $LaMnO_3$, Phys. Rev. B **60**, 7309 (1999).

[28] J. A. Alonso, M. J. Martínez-Lope, M. T. Casais, and M. T. Fernández-Díaz, Evolution of the Jahn-Teller distortion of MnO_6 octahedra in $RMnO_3$ perovskites (R = Pr, Nd, Dy, Tb, Ho, Er, Y): A neutron diffraction study, Inorg. Chem. **39**, 917 (2000).

[29] D. I. Khomskii, *Transition Metal Compounds* (Cambridge University Press, Cambridge, 2014).

[30] M. Daghofer, A. M. Oleś, and W. von der Linden, Orbital polarons versus itinerant e_g electrons in doped manganites, Phys. Rev. B **70**, 184430 (2004).

[31] Q. Huang, A. Santoro, J. W. Lynn, R. W. Erwin, J. A. Borchers, J. L. Peng, and R. L. Greene, Structure and magnetic order in undoped lanthanum manganite, Phys. Rev. B **55**, 14987 (1997).

[32] A. D. Becke, Density-functional thermochemistry: III. The role of exact exchange, J. Chem. Phys. **98**, 5648 (1993).

[33] P. J. Stephens, F. J. Devlin, C. F. Chabalowski, and M. J. Frisch, *Ab initio* calculation of vibrational absorption and circular dichroism spectra using density functional force fields, J. Chem. Phys. **98**, 11623 (1994).

[34] J. Zaanen and A. M. Oleś, Canonical perturbation theory and the two-band model for high-T_c superconductors, Phys. Rev. B **37**, 9423 (1988).

[35] W. A. Harrison, *Elementary Electronic Structure* (World Scientific, Singapore, 2005).

[36] A. E. Bocquet, T. Mizokawa, T. Saitoh, H. Namatame, and A. Fujimori, Electronic structure of 3d-transition-metal compounds by analysis of the 2p core-level photoemission spectra, Phys. Rev. B **46**, 3771 (1992).

[37] P. Czarnik, J. Dziarmaga, and A. M. Oleś, Overcoming the sign problem at finite temperature: Quantum tensor network for the orbital e_g model on an infinite square lattice, Phys. Rev. B **96**, 014420 (2017).

[38] F. Moussa, M. Hennion, J. Rodríguez-Carvajal, H. Moudden, L. Pinsard, and A. Revcolevschi, Spin waves in the antiferromagnet perovskite $LaMnO_3$: A neutron-scattering study, Phys. Rev. B **54**, 15149 (1996); G. Biotteau, M. Hennion, F. Moussa, J. Rodríguez-Carvajal, L. Pinsard, A. Revcolevschi, Y. M. Mukovskii, and D. Shulyatev, Approach to the metal-insulator transition in $La_{1-x}Ca_xMnO_3$ ($0 <\sim x <\sim 0.2$): Magnetic inhomogeneity and spin-wave anomaly, *ibid.* **64**, 104421 (2001).

[39] Y. Murakami, J. P. Hill, D. Gibbs, M. Blume, I. Koyama, M. Tanaka, H. Kawata, T. Arima, Y. Tokura, K. Hirota, and Y. Endoh, Resonant X-Ray Scattering from Orbital Ordering in $LaMnO_3$, Phys. Rev. Lett. **81**, 582 (1998).